ELSEVIER

Contents lists available at ScienceDirect

Materials Today Communications

journal homepage: www.elsevier.com/locate/mtcomm





Development and characterization of Forcespinning® mesquite gum nanofibers

Cristobal Rodriguez ^a, Victoria Padilla ^b, Karen Lozano ^b, Alexa Villarreal ^b, Luis Materon ^a, Robert Gilkerson ^{a,c,*}

- a Departments of Biology and Medical Laboratory Sciences, The University of Texas Rio Grande Valley, Edinburg, TX. USA
- ^b Mechanical Engineering, The University of Texas Rio Grande Valley, Edinburg, TX. USA
- ^c Mediical Laboratory Sciences, The University of Texas Rio Grande Valley, Edinburg, TX. USA

ARTICLE INFO

Keywords: Prosopis glandulosa Mesquite Gum Nanofibers Forcespinning® Antibacterial Biodegradable polymers

ABSTRACT

In this study, nanofibers incorporating *Prosopis glandulosa* mesquite gum (MG) exudate combined with biodegradable polymers, pullulan (PL) and chitosan (CH), were produced via the Forcespinning® technique. The nonwoven composite membranes were characterized via scanning electron microscopy followed by thermogravimetric and Fourier-transform infrared spectroscopy analysis. MG nanofiber composites comprised long, continuous fibers with an average fiber diameter of 523 ± 180 nm and 760 ± 225 nm for 18.1 and 28 wt% of MG, respectively. These composite membranes were water-stable after crosslinking via heat treatment with a ~ 3 % water absorption capacity, and demonstrated a thermal capability with an increasing residual weight of ~ 4 % near 900 °C at an increasing MG concentration. After 24 hr bacterial growth analysis, MG composite fiber based membranes show antibacterial properties against *E. coli* and *B. megaterium* bacteria with inhibition zones of 11 and 10 mm, respectively. Here, the successful incorporation of naturally-derived MG exudate into nanofiber systems was demonstrated, for potential utilization as a natural alternative for wound healing purposes.

1. Introduction

Advancements in nanoscale materials have demonstrated their material durability and thermal stability for the possible incorporation of protein or chemical cue markers [1]. The capacity of nanofiber materials for protein binding and impregnation techniques as drug delivery systems hold strong potential towards improved wound healing process [2]. Current nanofiber structures display characteristics similar to the extracellular matrix (ECM) [1], which functions as a supportive fibrous environment for cells in vivo, promoting the exchange of nutrients, waste, and fibroblast collagen secretion [3]. Various nanofiber compositions have demonstrated the use of biodegradable polymers incorporating a range of particle types. Previous findings have demonstrated the successful inclusion of silver nanoparticles in chitosan-based nanofibers with an antibacterial capability [4]. Fibers with a combination of surface-integrated zinc oxide nanoparticles in poly(D, L-lactic acid) and poly(3-hydroxybutyrate) allowed the growth of pre-osteoblast cells [5]. Further, Boyle et al. [6] determined that ternary composite nanofibers $(\sim 300-600 \text{ nm in fiber diameter})$ [7], [8] were effective in the removal of inflammatory chemokines, which could improve wound treatment within recessive dystrophic epidermolysis bullosa patients. These findings suggest that composite nanofibers may be used for improving wound healing, with the potential for inclusion of bioactive components to aid the process. Natural, plant-based materials provide a possible approach for inclusion of bioactive factors in composite nanofibers.

Electrospinning has been used with natural plant-based materials in conjunction with physiochemical compounds for different applications [9–14]. Bakhsheshi-Rad et al. [15], has previously shown an interesting natural silk-based nanofiber composition for wound healing application, demonstrating proof of principle for the use of natural components in nanofiber production. Similarly, development of plant-based nanofibers through Forcespinning® (FS), allows efficient production and high fiber yield via centrifugal force as previously shown [7], [16], [17]. These plant-based materials, developed from collected biomass, are found in seeds, flowers, leaves, and even roots [9], [11], [14], [18]. Such materials have also been described as 'smart materials' due to an applied plant mimicking behavior for sensing and physical change characteristics [19]. From a natural plant content, multiple physiochemical

^{*} Corresponding author at: Departments of Biology and Medical Laboratory Sciences, The University of Texas Rio Grande Valley, Edinburg, TX. USA. *E-mail address:* robert.gilkerson@utrgv.edu (R. Gilkerson).

Table 1 Component amounts used in a polymer solution preparation for nanofiber development. ((—) = 0 mg/g).

Sample	CA 1.41 wt % (mg)	CH 1.05 wt % (mg)	PL 9.05 wt % (mg)	MG 28 wt% (g)	DI water (mL)
PL	95	_	608	_	6
LMG-	150	_	900	2	8
18.1*					
JMG-28	-	-	876	2.8	6
PL/MG-28	138	-	890	2.8	6
CH/PL/	140	104	900	2.8	6
MG-28					

Different wt% and solvent volume were used for a lower concentration.

compounds are present with an unaltered composition, where a simplified extraction could prevent molecular disruption [7]. The incorporation of naturally-derived bioactive compounds through FS fiber production would enable the production of fibers with bioactive functional properties. Here, we explore the incorporation of mesquite gum (MG), a plant species with multiple potential bioactive components, into Forcespinning-produced nanofibers.

Prosopis glandulosa (honey mesquite) is an abundant native plant species in North and South America, with the ability to resist extreme weather conditions [20-22]. Prosopis spp. gum has demonstrated beneficial effects in multiple applications due to its capability as an emulsifying agent, encapsulation, fibril forming, and antibacterial abilities [23]. Plant gum exudate is known to contain carbohydrates such as D-galactose, L-arabinose, and D-mannose [21], [24-28]. The presence of antioxidants, alkaloids, and flavonoid content has been demonstrated in *Prosopis* gum as well [23], [29]. Previous studies have shown the full development of fibers within the incorporation of different *Prosopis* spp. and other plant gum exudate [12], [21], [30–33], with antibacterial and cell growth capabilities [13], [33]. However, the usage within material development and biological studies of P. glandulosa gum exudate, a native species in Texas and Mexico, remains unexplored. The possible incorporation of mesquite gum (MG) in composite nanofibers would further expand our understanding of P. glandulosa's capabilities and its application for wound healing.

Here, we explore the fabrication of FS composite nanofibers containing chitosan (CH), pullulan (PL), and *P. glandulosa* MG exudate as a potential bioactive additive. MG composite nanofibers incorporating varying concentrations of MG and PL were characterized via scanning electron microscopy (SEM), a thermogravimetric analysis (TGA), and Fourier-transform infrared spectroscopy (FT-IR) analysis. Additionally, an antibacterial evaluation with Gram-negative *Escherichia coli* (MM 294) and Gram-positive bacteria *Bacillus megaterium* (ATCC 14581) was conducted via disk diffusion. Our results demonstrate that FS-produced nanofibers allow for the incorporation of naturally-derived plant-based components with complete structural integrity, further motivating the potential of these fibers for functional applications in biological studies.

2. Materials and method

2.1. Materials

Low molecular weight (50–190 kg·mol-1, based on viscosity) chitosan (CH) and citric acid (CA) were purchased from Sigma-Aldrich®. Pullulan (PL) (P0978) was purchased from Tokyo Chemical Industry Co. Ltd. (TCI). Deionized water (DI) (18.20 M Ω cm) used for this study was filtered through Barnstead MicroPure ST® (Thermo Fisher Scientific).

2.2. P. glandulosa gum collection

MG exudate gum was acquired and collected from a + 20-year-old mesquite (*P. glandulosa*) tree (origin: Edinburg, Texas) standing \sim 3 m tall while following similar separation and filtration procedures as

previously described [7]. Bark and debris trapped in MG were removed by crushing with a pestle in a mortar. After weighing the crushed MG sample, the sample was combined with DI water in a 50 mL centrifuge tube, and left overnight sealed with parafilm for complete dissolution at 4 °C for preservation. MG solution was then centrifuged for 10 min at 9000 rpm to further separate debris content. MG supernatant was then collected with a 3 mL plastic syringe and filtered using a 0.22 μm size syringe filter.

2.3. Solution preparation

Table 1 displays the components and amounts used in the polymer solution preparation. Control sample preparation began by adding 608 mg of PL in a CA aqueous solution (CA 95 mg/6 mL DI water) to produce a PL concentration of 9.05 wt%. The solution was then vortexed and left stirring for 2 h until reaching full homogenization. A low MG concentration system (LMG-18.1), was prepared introducing 2 g of MG extract (MG 2 g/2 mL of DI) in a previous PL/CA solution combination in DI water to obtain a system with 18.1 wt% of MG. In a separate assessment a high concentration of MG extract (28 wt%) was evaluated without CA to determine the effects on crosslinking within the combination of just MG with PL, represented by JMG-28. Similar polymer concentrations were used at 28 wt% MG with PL into CA solution, PL/MG-28. To further explore material stability, 104 mg of CH were combined with the CA solution (CA 140 mg/3 mL of DI water) and left stirring overnight; 900 mg of PL was then added into CA/CH prepared solution, left stirring for 2 h, and vortexed until fully dissolved. When the solution was well dispersed, 2.8 g of filtered MG was incorporated to obtain 28 wt% MG in the final solution, as represented by CH/PL/MG-28.

2.4. Nanofiber production

Control PL, LMG-18.1, JMG-28, PL/MG-28, and CH/PL/MG-28 nanofiber samples were spun at low (29–53 %) relative humidity levels at 7000 rpm via FS on a CycloneTM L-1000 M (FibeRio Technology, Corp.) equipped with a two nozzle cylindrical spinneret. Fiber production was conducted by injecting 1.5 mL of prepared polymer solution, with a 3 mL plastic syringe, into spinneret and released through centrifugal force as fine solution jets, producing fibers through solvent evaporation. These fibers were deposited onto ten collector columns placed 4.5 in. apart around the spinneret at an 8-inch distance. Nanofibers were collected with an aluminum-covered frame, followed by crosslinking at $\sim\!145\,^{\circ}\mathrm{C}$ for 1 h.

2.5. Nanofiber characterization

For nanofiber morphology, PL (control), LMG-18.1, JMG-28, PL/MG-28, and CH/PL/MG-28 nanofiber membranes were cut into $\sim 5~\text{mm}\times 5~\text{mm}$ mats, sputtered coated with gold, and analyzed through a scanning electron microscope (SEM) (Carl Zeiss, SigmaVP). Using ImageJ 1.50i software, 300 fiber measurements per sample helped determine average fiber diameter. A thermogravimetric analysis (TGA) (TG 209 $_{\rm F3}$ Tarsus@ NETZSCH) determined both polymer and material thermal degradation patterns. For a TGA, nanofiber samples weighing $\sim \! 10~\text{mg}$ were heated on an alumina crucible from 25° to 900°C at a heating rate of 10 K/min under inert nitrogen gas flow. Fourier transform infrared spectroscopy (FTIR) (VERTEX 70 v FTIR Spectrometer, Bruker®) analysis was conducted in transmittance mode (4000–400 cm $^{-1}$) for all samples.

2.6. Water stability analysis

To determine water stability of the developed MG composite nanofibers, samples were submerged in DI water. Nanofiber samples were cut into 2 in \times 1 cm ($l \times w$) strips and taped from end to end onto a glass slide for viewing under a contact angle meter (KYOWA© DropMaster). Further analysis was initiated by submerging 1 cm \times 1 cm nanofiber

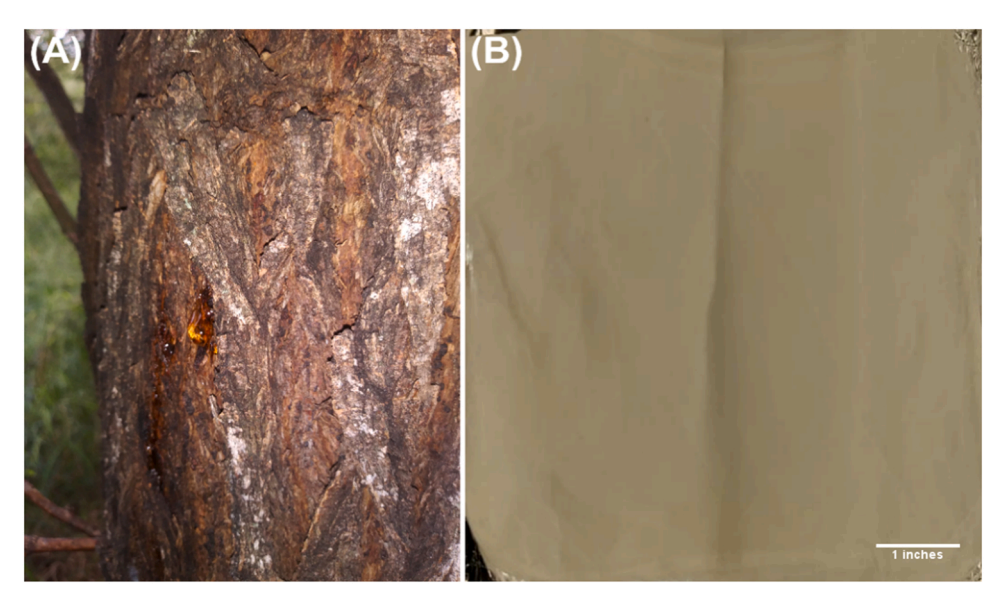


Fig. 1. Prosopis glandulosa (honey mesquite) (A) and 5×5 in. MG nanofiber mats (B).

samples into 10 mL of DI water for 1 hr. Samples were then lifted and airdried for 24 hr, followed by sputter coating with gold for viewing under the SEM. A water absorption analysis was determined by leaving PL/MG-28 composites submerged in DI water with filter paper for 20, 30, and 60 min time points. Prior submerging samples in DI water, a dry weight was recorded for an initial weight (W_i). Once samples were submerged and removed for drying, an air-dried sample weight was used to represent its final weight (W_f) to calculate for a percentage water absorption capacity, as shown in Eq. (1) [7], [32], [34].

Water absorption capacity (%) =
$$[(W_f - W_i)/W_i] \times 100$$
 (1)

2.7. Antibacterial study

Gram-negative *Escherichia coli* (MM 294) and Gram-positive bacteria *Bacillus megaterium* (ATCC 14581) were tested via disk diffusion. $100~\mu Ls$ of bacterial cell suspension from a $1~\times~10^6/mL$ culture were placed individually onto Mueller-Hinton agar plates. Nanofiber samples were cut into disk shapes of 1 cm in diameter, then laid onto individual spread *E. coli* and *B. megaterium* cultures and incubated at 37 °C for 24 hrs. The presence of MG was further analyzed by placing five drops of sterilized MG solution (1:1 ratio of MG/DI water) onto individual agar plates and incubated for 24 hr. Before incubation, brief centrifugation was used to remove debris, filtered, heat-treated in an oven at 60 °C, and then UV-light sterilized for 10 min. After incubation, the observed zone of inhibition for each was recorded.

3. Results and discussion

3.1. Nanofiber production and characterization

MG composed nanofibers were successfully generated through the FS technique, with different MG concentrations used alongside the combination of CA and CH for thermal crosslinking treatment, while PL provided fibril capability for LMG-18.1, JMG-28, PL/MG-28, and CH/PL/MG-28 (Fig. 1A,B). Nanofiber SEM micrographs in Fig. 2a-e showed long continuous fiber structures, with some particle agglomerations obtained for all samples at different MG concentrations. Fig. 2f-j demonstrates the fiber size distribution and statistical significance (**p <0.01) between all samples, where control PL displayed an average fiber diameter ($\underline{D_f}$) of 247 \pm 97 nm and LMG-18.1 with an $\underline{D_f}$ of 523

 \pm 180 nm. JMG-28, PL/MG-28, and CH/PL/MG-28 showed an $\underline{D_f}$ of 637 \pm 233 nm, 760 \pm 225, and 681 \pm 182 nm, respectively. A slight increase in fiber diameter is displayed as MG concentration is increased. This change is likely due to the viscosities of MG [20], [21], [32] and polymer combination [7], influencing the average nanofiber diameter and its distribution between samples.

3.2. Water stability analysis

Fig. 3a,b shows a side view contact angle. Pendant drop method was used for water contact analysis to examine surface interaction between DI water and nanofiber samples. In a DI water drop-fiber interaction, the water was absorbed immediately by the fibers. This interaction demonstrates the hydrophilic behavior of these nanofiber systems. Samples LMG-18.1, PL/MG-28, and CH/PL/MG-28 were followed by submerging into DI water, then removed and air-dried. After the water treatment, the nanofiber supportive structure remained undisturbed, while also displaying swollen fibers (Fig. 3c). A water absorption capacity analysis was then conducted to further evaluate both swelling characteristics and water interactions within PL/MG-28. An initial weight was recorded from a dry PL/MG-28 nanofiber sample. Submerged in DI water with a filter paper as previously described [34], then air-dried where a final weight was measured. Once PL/MG-28 nanofibers were removed and dried a 5.84 %, 5.65 %, and 3.76 % water absorption capacity was demonstrated after 20, 30, 60 mins, respectively (p > 0.05). Further demonstrating a constant performing adequate water retaining capability. Through crosslinking between hydroxyl and carboxylic groups [7], water stability is made possible with the introduction of CA and PL; as such, JMG-28 composite nanofibers have higher solubility due to CA being omitted from the composition. Within a fluid-based environment, both a hydrophilic and hydrophobic interaction is described for materials to display a stable condition for an appropriate biological functional system [1].

3.3. Thermal degradation analysis

The degradation patterns of developed nanofibers containing different concentrations of MG exudate are presented in Fig. 4. All systems displayed an initial weight loss due to water evaporation characteristics within the range of $100\,^{\circ}$ C, at a loss of $11.03\,\%$, $7.53\,\%$, $7.32\,\%$, $5.97\,\%$, and $8.6\,\%$ for control PL, LMG-18.1, JMG-28, PL/MG-28, and

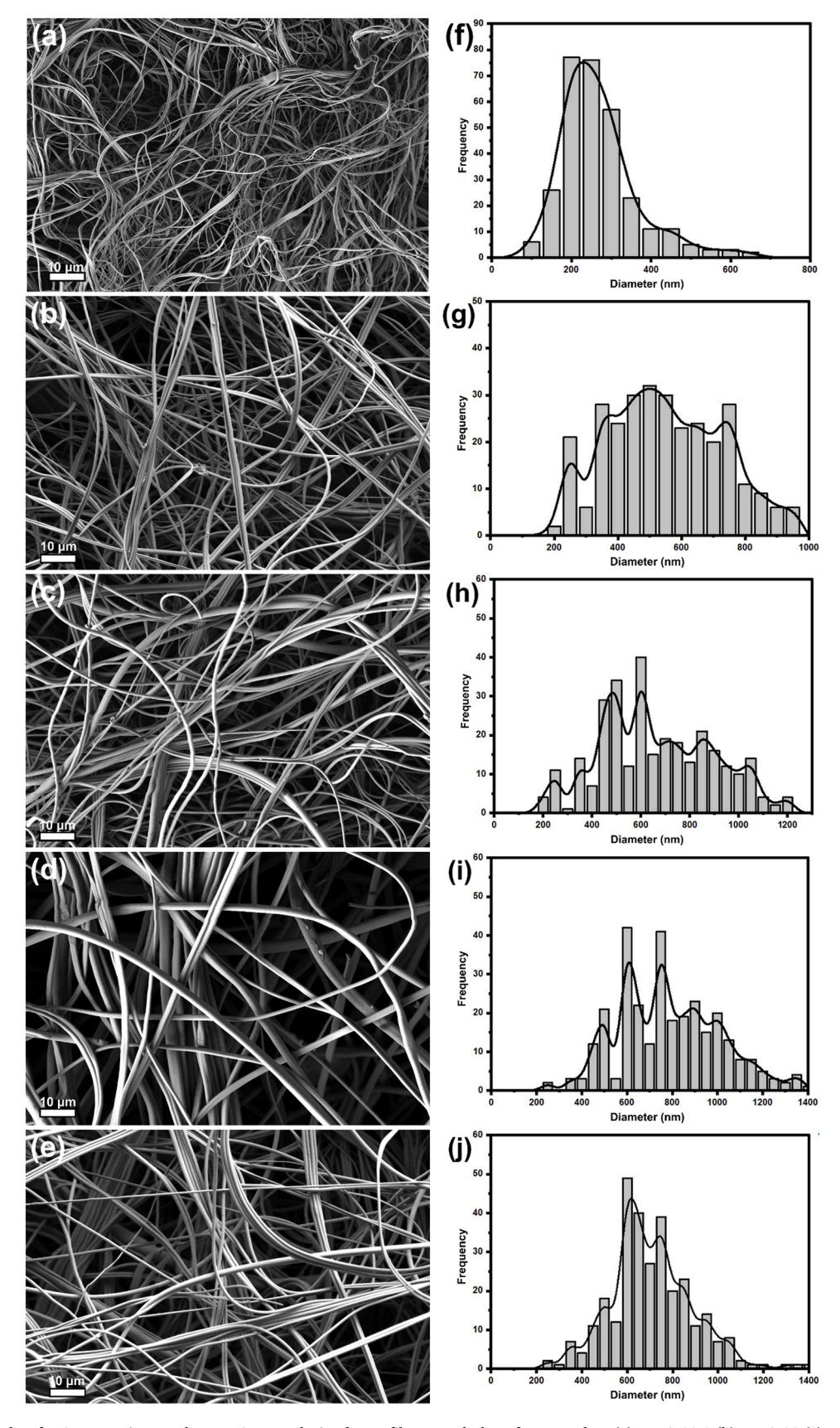


Fig. 2. SEM micrographs of MG composite membranes: SEM analysis of Nanofiber morphology for control PL (a), LMG-18.1 (b), JMG-28 (c), PL/MG-28 (d), and CH/PL/MG-28 (e) nanofibers are shown. Scale bar = $10 \mu m$. Fiber diameter distribution is shown for control PL (f), LMG-18.1 (g), JMG-28 (h), PL/MG-28 (i), and CH/PL/MG-28 (j). Sample size: n = 300. One-way ANOVA post-hoc Tukey's test demonstrated significant difference between samples (** p < 0.01).

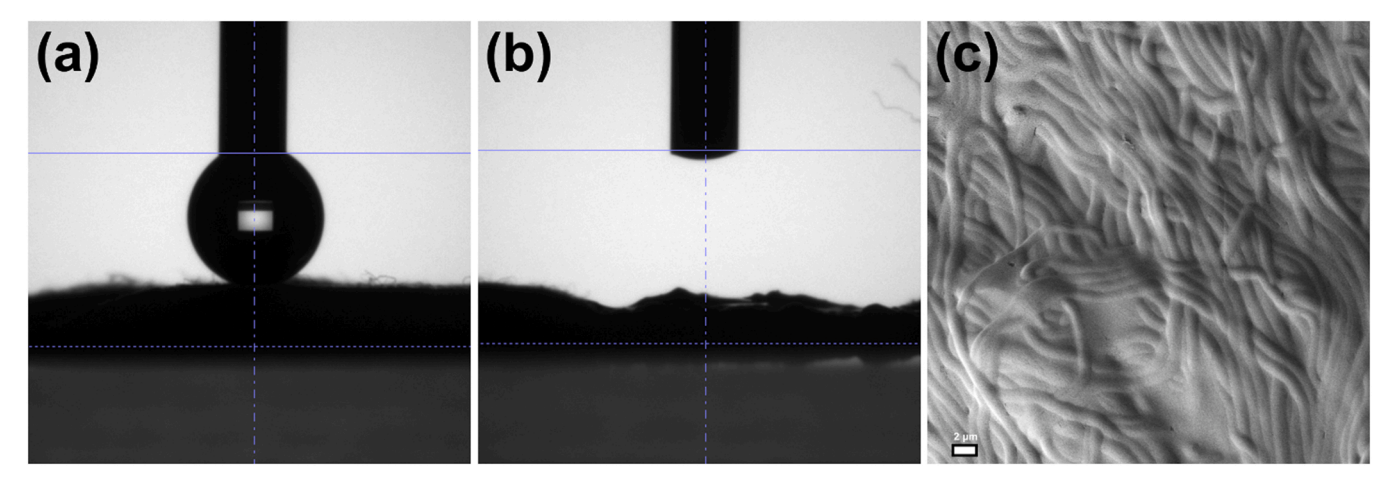


Fig. 3. Material hydrophilic interactions and water stability: Images display an initial DI water drop contact onto material (a), a quick DI drop absorption (b), and an SEM micrograph from a dry PL/MG-28 nanofiber sample after being submerged in DI water (c). Scale bar $= 2 \mu m$.

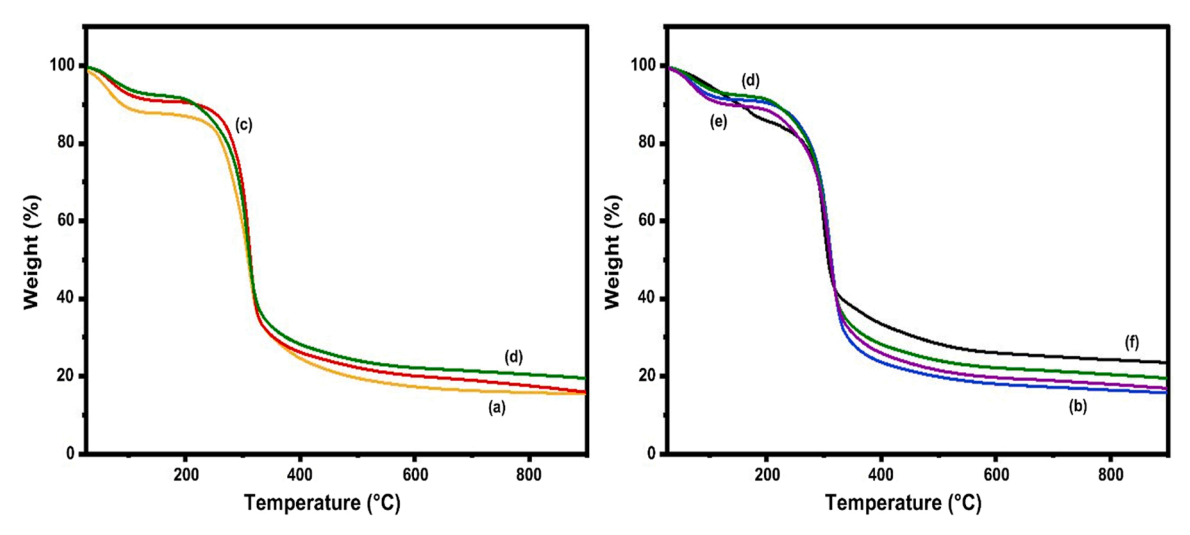


Fig. 4. TGA analysis of composite nanofibers: TGA weight (%) loss is displayed for nanofiber samples control PL (a), LMG-18.1 (b), JMG-28 (c), PL/MG-28 (d), CH/PL/MG-28 (e), and raw MG exudate (f).

CH/PL/MG-28, respectively. TGA of a raw MG sample showed initial weight loss of 11.32 % at 165 °C. Within the second degradation stage, a \sim 5 % mass loss of weight was shown for the raw MG sample at 220 °C. where a glass transition was previously shown to occur further at 230 °C from a mesquite gum sample [21], [28]. A similar result found by Basu et al. [30] was demonstrated, where TGA analysis of gum exudate displayed a weight loss due to both water evaporation around 100 °C and degradation of polysaccharides at 260 °C. Similar material degradation patterns were present with a lower weight loss at a higher polymer concentration presence attributed to pullulan and chitosan [7]. In samples LMG-18.1, JMG-28, PL/MG-28, and CH/PL/MG-28, a secondary degradation pattern at 320 °C with a ~50 % weight loss was displayed. This loss is consistent with MG exudate thermograph reported by Basu et al. [30], where 39.77 % residual weight loss was shown at 310 °C along with final carbonization. Further, samples presented higher thermal stability, with consistent decomposition rate above \sim 600 °C within a presence of MG, where a final reaction could be due to remaining polysaccharide components [23]. A higher residual weight was displayed with an increasing MG concentration, specifically ~15.45 %, 15.69 %, 15.89 %, 19.49 %, 16.88 %, and 23.51 % for control PL, LMG-18.1, JMG-28, PL/MG-28, CH/PL/MG-28, and MG sample, respectively. Through the final degradation patterns of MG composites, an improved thermal stability can be observed compared to control PL

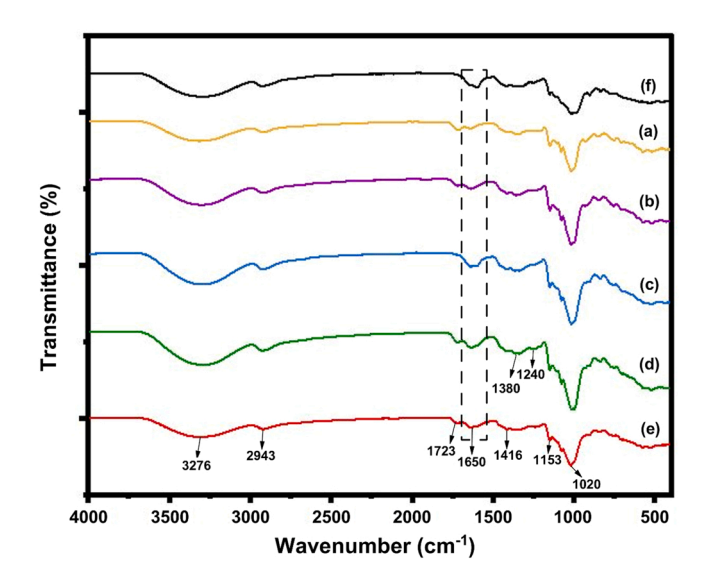


Fig. 5. FTIR analysis of Nanofibers at increasing concentration of MG: FTIR spectrum of nanofiber control PL (a), LMG-18.1 (b), JMG-28 (c), PL/MG-28 (d), CH/PL/MG-28 (e), and raw MG (f) sample.

Table 2 Mean \pm standard deviation (SD) diameter zone of inhibition measurements are shown for LMG-18.1, JMG-28, PL/MG-28, and CH/PL/MG-28 against *E. coli* and *B. megaterium*. ((—) = no value; n = 3 sample size).

Zone of Inhibition (mm)	LMG- 18.1	JMG- 28	PL/MG-28	CH/PL/MG- 28
E. coli	-	-	11.33 ± 1.15	-
B. megaterium	_	-	10 ± 0	_

nanofibers even after the crosslinking heat treatment process, as shown due to the possible carbonization of residual MG protein and mineral content [22].

3.4. FTIR analysis

Fig. 5 displays the FTIR spectrums for PL (control), LMG-18.1, JMG-18.1, PL/MG-28, CH/PL/MG-28, and raw MG exudate to examine the effect of MG at variant concentrations. Throughout all spectra, polymer and plant-based polysaccharide characteristics could be identified through different functional groups such as carboxylic acid, ether, amide, and alcohol groups, as previously described [7]. The broad bands within the range of 3600-3000 cm⁻¹ correspond to hydrogen-bonded O-H stretches from alcohol and carboxylic acid-OH groups, where interaction between polysaccharides and water occurs. This interaction is present in all systems with an increasing presence in MG concentration. Bands around 2940 cm⁻¹ related to the vibrations of CH and CH₂ groups were identified as previously described [7], [35]. A C=O stretching vibration from carboxylic groups at $1723 \ cm^{-1}$ is demonstrated; showing a higher intensity as the MG concentration increases. A band shift shown at 1650 cm⁻¹ from a ~1588 cm⁻¹ corresponds to an amide I attributed to protein presence, and C=O vibration of amino acid described for Prosopis spp. gum [23], [36]. The apparent shifts in LMG-18.1, PL/MG-28, and CH/PL/MG-28 could be due to the possible interactions of hydroxyl and carboxylic groups, where narrowing peaks are present due to a lack of CA in JMG-28 composites. A COO-

asymmetric stretch of MG was demonstrated around 1416 cm⁻¹ [13]. The bands at 1380 cm⁻¹ and 1240 cm⁻¹ likely correspond to C=O stretching of esters from polysaccharides and hydroxyl groups [7], [23]. The presence of carbohydrates is present around a final transmittance band at 1153 cm⁻¹ and ~1020 cm⁻¹ attributing to C-O and C-O-H vibrations, respectively [36]. In a previous study, MG characteristics were demonstrated through a UV-absorbance within the range wavenumber of 200–800 nm, where a *Prosopis* spp. xylose and glucose (an abundant plant carbohydrate) was present with an absorbance signal at 210 nm and 265 nm [23]. As concentration increased, MG composites further demonstrated the conservation of polysaccharides and other functional groups after crosslinking.

3.5. Antibacterial study

In Table 2, inhibition zone measurements are presented (diameter in mm). After a 24 hr incubation, no inhibition was found for control PL (Fig. 6), LMG-18.1, JMG-28, or CH/PL/MG-28 against E. coli and B. megaterium cultures. The absence of an inhibition zone in these samples may correlate with an excluded MG and lower concentration of MG in PL nanofibers and LMG, while also showing a reduced effect against bacteria with a lack of CA found in JMG. The lack of bacterial inhibition for CH/PL/MG-28 could be due to a reduced appropriate fiber distribution; where within a developed mat a wider fiber distribution could present a greater porosity (i.e. interfiber space) and therefore greater surface area with greater effectiveness in a fibrous system. In the presence of PL/MG-28, a small zone of inhibition against E. coli is apparent due to the higher concentration of MG and wider fiber distribution (Fig. 6). Samrot et al. [23] demonstrate similar results, where a minimal bacterial inhibition is present from 2 mg of *Prosopis* spp. gum against S. aureus [29] and Bacillus spp. In a separate evaluation of MG against bacteria, both E. coli and prolific B. megaterium showed an inability to spread into the areas where MG solution had been applied (Fig. 6). These inhibitory capabilities of MG are likely due to the presence of tannins derived from the bark of mesquite [22], which disrupts the bacterial cell membrane and blocks the metabolic activity of bacteria

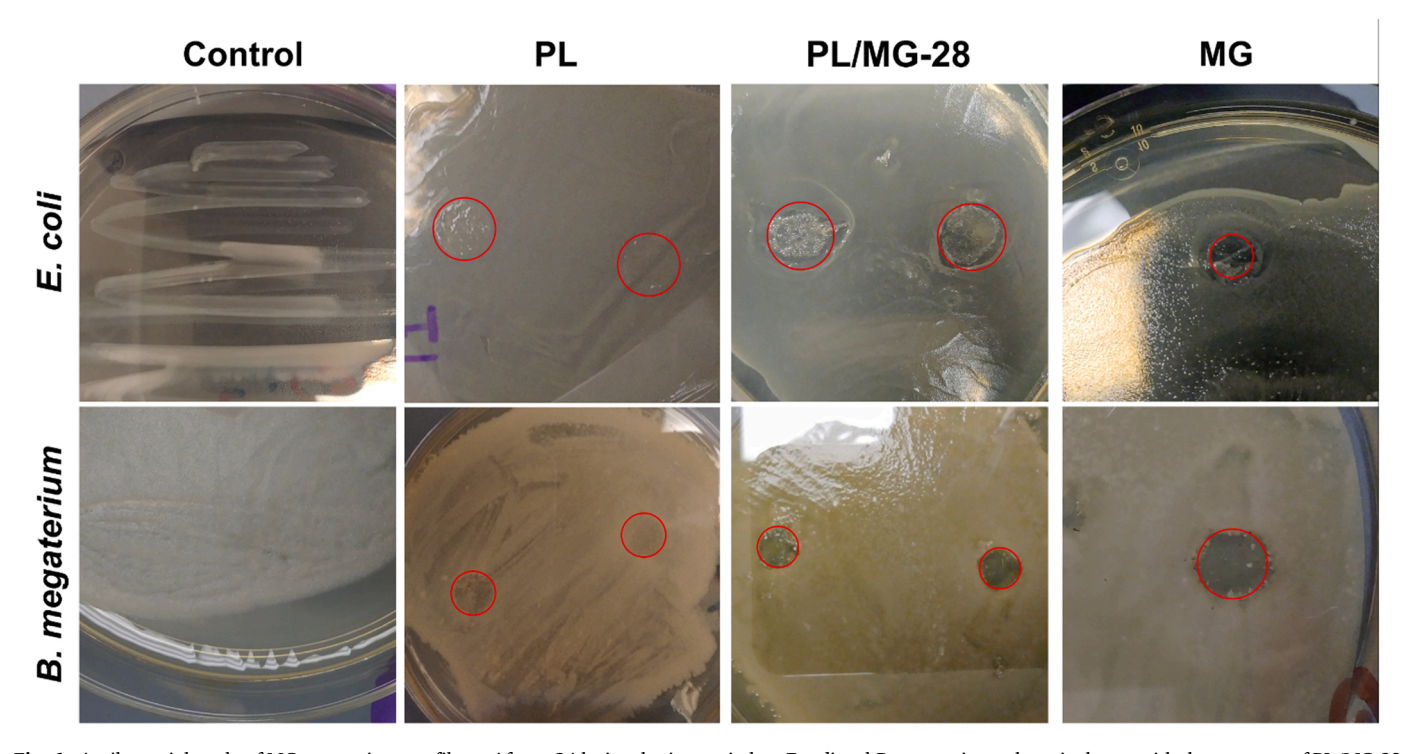


Fig. 6. Antibacterial study of MG composite nanofibers: After a 24 hr incubation period an *E. coli* and *B. megaterium* culture is shown with the presence of PL/MG-28 composites and MG solution. Red circles are indicated for control PL samples, and for both PL/MG-28 and MG solution inhibition zones.

[29], [37], [38]. MG incorporation demonstrates a promising antibacterial capability against Gram-negative bacteria and possible prevention of spore-forming bacteria, further motivating the introduction of MG composites in other biological studies.

4. Conclusion

Here, we demonstrate the successful use of Forcespinning® for the development of composite nanofibers incorporating *P. glandulosa* MG exudate. At an increasing MG concentration, nanofiber membranes consisted of long continuous fibers and a porous three-dimensional supportive structure similar to the ECM. The developed MG-containing nanofibers exhibited an interactive water capability while maintaining structural integrity due to crosslinking. Further, the integration of MG within these nanofiber systems demonstrated both thermal stability and bacterial inhibition, likely due to phenolic compounds. *P. glandulosa* (honey mesquite) provides an ample production of gum exudate with naturally-occurring bioactive content. These findings further motivate the exploration of MG, as well as other bioactive naturally-derived components, for incorporation within nanoscale materials for future studies in mammalian cell growth studies.

CRediT authorship contribution statement

Cristobal Rodriguez: Conceptualization, Methodology, Validation, Investigation, Writing – original draft. Victoria Padilla: Validation, Investigation, Writing – review & editing. Karen Lozano: Resources, Writing – review & editing, Funding acquisition. Alexa Villarreal: Investigation, Writing – review & editing. Luis Materon: Validation, Resources. Robert Gilkerson: Supervision, Resources, Writing – review & editing.

Declaration of Competing Interest

The authors declare that they have no known competing financial interests or personal relationships that could have appeared to influence the work reported in this paper.

Data Availability

Data will be made available on request.

Acknowledgements

The authors gratefully acknowledge support received by NSF PREM award under grant No. DMR-2122178: UTRGV-UMN Partnership for Fostering Innovation by Bridging Excellence in Research and Student Success (to K. L.).

References

- T.L. Jenkins, D. Little, Synthetic scaffolds for musculoskeletal tissue engineering: cellular responses to fiber parameters, npj Regen. Med. 4 (2019) 15, https://doi. org/10.1038/s41536-019-0076-5.
- [2] M. Hajialyani, D. Tewari, E. Sobarzo-Sanchez, S.M. Nabavi, M.H. Farzaei, M. Abdollahi, Natural product-based nanomedicines for wound healing purposes: therapeutic targets and drug delivery systems, Int. J. Nanomed. 13 (2018) 5023–5043. https://doi.org/10.2147/JJN.S174072.
- [3] L. Sherwood, Human physiology from cells to systems Ninth Edition, 2016, pp. 404–442.
- [4] L. Cremar, J. Gutierrez, J. Martinez, L. Materon, R. Gilkerson, F. Xu, K. Lozano, Development of antimicrobial chitosan based nanofiber dressings for wound healing applications, Nanomed. J. 5 (1) (2018) 6–14. https://nmj.mums.ac.ir/article10049.html).
- [5] V. Padilla-Gainza, H. Rodríguez-Tobías, G. Morales, A. Ledezma-Pérez, C. Alvarado-Canché, C. Rodríguez, R. Gilkerson, K. Lozano, Processing-structureproperty relationships of biopolyester/zinc oxide fibrous scaffolds engineered by centrifugal spinning, Polym. Adv. Technol. 31 (2020) 2601–2614, https://doi.org/ 10.1002/pat.4987.

- [6] W. Boyle, W. Chen, A. Rodriguez, S. Linn, J. Tolar, K. Lozano, T. Reineke, Ternary composite nanofibers containing chondroitin sulfate scavenge inflammatory chemokines from solution and prohibit squamous cell carcinoma migration, ACS Appl. Bio Mater. 2 (2) (2019) 619–624, https://doi.org/10.1021/acsabm.8b00690.
- [7] C. Rodriguez, V. Padilla, K. Lozano, A. McDonald, L. Materon, A. Chapa, F. Ahmad, C. Trevino De Leo, R. Gilkerson, Fabrication of Forcespinning® nanofibers incorporating nopal extract, Polym. Int. 70 (2020) 679–686, https://doi.org/10.1002/pi.6163.
- [8] F. Xu, B. Weng, R. Gilkerson, L. Materon, K. Lozano, Development of tannic acid/chitosan/pullulan composite nanofibers from aqueous solution for potential applications as wound dressing, Carbohydr. Polym. 115 (2015) 16–24, https://doi.org/10.1016/j.carbpol.2014.08.081.
- [9] S. Ahn, H.A.M. Ardona, P.H. Campbell, G.M. Gonzalez, K.K. Parker, Alfalfa nanofibers for dermal wound healing, ACS Appl. Mater. Interfaces 11 (2019) 33535–33547, https://doi.org/10.1021/acsami.9b07626.
- [10] U. Dashdorj, M.K. Reyes, A.R. Unnithan, A.P. Tiwari, B. Tumurbaatar, C.H. Park, C. S. Kim, Fabrication and characterization of electrospun zein/Ag nanocomposite mats for wound dressing applications, Int. J. Biol. Macromol. 80 (2015) 1–7, https://doi.org/10.1016/j.ijbiomac.2015.06.026.
- [11] P. Golkar, A. Allafchian, B. Afshar, Alyssum lepidium mucilage as a new source for electrospinning: production and physicochemical characterization, IET Nanobiotechnol. 12 (3) (2017) 259–263, https://doi.org/10.1049/ietnbt.2017.0133.
- [12] H.M. Mohammed, M.H. Taiseer, A.A.A. Youssif, Production of fiber from mesquite plant (Prosopis juliflora. L.), IJEAS 6 (9) (2019), https://doi.org/10.31873/ IJEAS.6.9.18. ISSN: 2394-3661.
- [13] M. Ranjbar-Mohammad, S.H. Bahrami, M.T. Joghataei, Fabrication of novel nanofiber scaffolds from gum tragacanth/poly(vinyl alcohol) for wound dressing application: In vitro evaluation and antibacterial properties, Mater. Sci. Eng. C. 33 (2013) 4935–4943, https://doi.org/10.1016/j.msec.2013.08.016.
- [14] H. Urena-Saborio, E. Alfaro-Viquez, D. Esquivel-Alvarado, S. Madrigal-Carballo, S. Gunasekaran, Electrospun plant mucilage nanofibers as biocompatible scaffolds for cell proliferation, Int. J. Biol. Macromol. 115 (2018) 1218–1224, https://doi. org/10.1016/j.ijbiomac.2018.04.129.
- [15] H.R. Bakhsheshi-Rad, A.F. Ismail, M. Aziz, M. Akbari, Z. Hadisi, M. Omidi, X. Chen, Development of the PVA/CS nanofibers containing silk protein sericin as a wound dressing: in vitro and in vivo assessment, Int. J. Biol. Macromol. 149 (2020) 513–521, https://doi.org/10.1016/j.ijbiomac.2020.01.139.
- [16] M. Akia, C. Rodriguez, L. Materon, R. Gilkerson, K. Lozano, Antibacterial activity of polymeric nanofiber membranes impregnated with Texas sour orange juice, Eur. Polym. J. 115 (2019) 1–5, https://doi.org/10.1016/j.eurpolymj.2019.03.019.
- [17] R. Barbosa, A. Villarreal, C. Rodriguez, H. De Leon, R. Gilkerson, K. Lozano, Aloe vera extract-based composite nanofibers for wound dressing applications, Mater. Sci. Eng. C. 124 (2021), 112061, https://doi.org/10.1016/j.msec.2021.112061.
- [18] F.M. Pelissari, M.M. Andrade-Mahecha, P.J. do Amaral Sobral, F.C. Menegalli, Nanocomposites based on banana starch reinforced with cellulose nanofibers isolated from banana peels, J. Colloid Interface Sci. 505 (2017) 154–167, https://doi.org/10.1016/j.icis.2017.05.106.
- [19] D. Lunni, M. Cianchetti, C. Filippeschi, E. Sinibaldi, B. Mazzolai, Plant-inspired soft bistable structures based on hygroscopic electrospun nanofibers, Adv. Mater. Interfaces 7 (2020) 1–8, https://doi.org/10.1002/admi.201901310.
- [20] Y.L. Lopez-Franco, R.E. Cordova-Moreno, F.M. Goycoolea, M.A. Valdez, J. Juarez-Onofre, J. Lizardi-Mendoza, Classification and physicochemical characterization of mesquite gum (*Prosopis* spp.), Food Hydrocoll. 26 (2012) 159–166, https://doi.org/10.1016/j.foodhyd.2011.05.006.
- [21] D. Mudgil, S. Barak, Mesquite gm (Prosopis gum): structure, properties & applications – a review, Int. J. Biol. Macromol. 159 (2020) 1094–1102, https://doi. org/10.1016/j.iibiomac.2020.05.153
- [22] K. Parveen, A.G.M. Vasandan, G. Zuhra-Memon, F. Memon, M.A. Moghal, Physicochemical characterization of gum exuded from prosopis cineraria and prosopis glandulosa species of Thar desert Pakistan, IOSRJEN 4 (12) (2014) 54–60, https://doi.org/10.9790/3021-0412254060.
- [23] A.V. Samrot, T. Kudaiyappan, U. Bisyarah, A. Mirarmandi, E. Faradjeva, A. Abubakar, J.A. Selvarani, S.K. Subbiah, Extraction, purification, and characterization of polysaccharides of Araucaria heterophylla L and Prosopis chilensis L and utilization of polysaccharides in nanocarrier synthesis, Int. J. Nanomed. 15 (2020) 7097–7115, https://doi.org/10.2147/IJN.S259653.
- [24] S. Cortes-Camargo, R. Gallardo-Rivera, B.E. Barragan-Huerta, O. Dublan-Garcia, A. Roman-Guerrero, C. Perez-Alonso, Exploring the potential of mesquite gumnopal mucilage mixture: physicochemical and functional properties, J. Food Sci. 83 (2018) 113–121, https://doi.org/10.1111/1750-3841.13937.
- [25] Y.L. Lopez-Franco, F.M. Gooycolea, J. Lizardi-Mendoza, Gum of Prosopis/Acacia species, Polysaccharides (2014) 1–20, https://doi.org/10.1007/978-3-319-03751-6141.
- [26] J. Orozco-Villafuerte, F. Cruz-Sosa, E. Ponce-Alquicira, E.J. Vernon-Carter, Mesquite gum: fractionation and characterization of the gum exuded from *Prosopis laevigata* obtained from plant tissue culture and wild trees, Carbohydr. Polym. 54 (2003) 327–333, https://doi.org/10.1016/S0144-8617(03)00187-5.
- [27] M.Z. Siddiqui, N. Prasad, J.C. Tewari, Physicochemical properties and toxicity test of Prosopis juliflora (Sw.) DC. and Balanites aegyptiaca Del gum exudates from Rajasthan, IJEB 55 (2017) 782–788. (http://nopr.niscpr.res.in/handle/12345678 9/43046).
- [28] F.E. Vasile, M.A. Judis, M.F. Mazzobre, Moisture sorption properties and glass transition temperature of a non-conventional exudate gum (*Prosopis alba*) from northeast Argentine, Food Res. Int. 131 (2020), 109033, https://doi.org/10.1016/ i.foodres.2020.109033.

- [29] J. Sharifi-Rad, F. Kobarfard, A. Ata, S.A. Ayatollahi, N. Khosravi-Dehaghi, A. K. Jugran, M. Tomas, E. Capanoglu, K.R. Mattews, J. Popovic-Djordjevic, A. Kostic, S. Kamiloglu, F. Sharopov, M.I. Choudhary, N. Martins, *Prosopis* plant chemical composition and pharmacological attributes: targeting clinical studies from preclinical evidence, Biomolecules 9 (12) (2019) 777, https://doi.org/10.3390/biom9120777.
- [30] S. Basu, M.N.V. Prasad, S. Suthari, B.R. Kiran, *Prosopis juliflora* (mesquite) gum exudate as a potential excipient, Eur. J. 1 (1) (2017) 76–81, https://doi.org/ 10.24190/JSSN2564-615X/2017/01 12
- [31] X. Zhang, X. Kang, L. Jin, J. Bai, W. Liu, Z. Wang, Stimulation of wound healing using bioinspired hydrogels with basic fibroblast growth factor (bFGF), Int. J. Nanomed. 13 (2018) 3897–3906, https://doi.org/10.2147/IJN.S168998.
- [32] A.C.S. Ferreira, R. Aguado, A.M.M.S. Carta, R. Bertolo, D. Murtinho, A.J. M. Valente, Insights into Gum Arabic interactions with cellulose: strengthening effects on tissue paper, Mater. Today Commun. 31 (2022), 103706, https://doi. org/10.1016/j.mtcomm.2022.103706.
- [33] A. Amirsadeghi, A. Jafari, S.-S. Hashemi, A. Kazemi, Y. Ghasemi, A. Derakhshanfar, M.-A. Shahbazi, S.V. Niknezhad, Sprayable antibacterial Persian gum-silver

- nanoparticle dressing for wound healing acceleration, Mater. Today Commun. 27 (2021), 102225, https://doi.org/10.1016/j.mtcomm.2021.102225.
- [34] K. Zhang, W. Feng, C. Jin, Protocol efficiency measuring the swelling rate of hydrogels, MethodsX 7 (2020), 100779, https://doi.org/10.1016/j. mex.2019.100779.
- [35] Y.L. Lopez-Franco, A.M.C. de la Barca, M.A. Valdez, M.G. Peter, M. Rinaudo, G. Chambat, F.M. Goycoolea, Structural characterization of Mesquite (Prosopis velutina) gum and its fractions, Macromol. Biosci. 8 (2008) 749–757, https://doi. org/10.1002/mabi.200700285.
- [36] M.B. Moreno-Trejo, M. Sanchez-Dominguez, Mesquite gum as a novel reducing and stabilizing agent for modified tollens synthesis of highly concentrated Ag nanoparticles, Materials 9 (2016) 817, https://doi.org/10.3390/ma9100817.
- [37] J.V. Kurhekar, TANNINS antimicrobial chemical components, Int. J. Technol. Sci. 9 (3) (2016) 5–9. https://scholar.google.com/scholar_lookup?journal=Int+J+Technol+Sci&title=Tannins-antimicrobial+chemical+components&author=JV+Kurhekar&volume=9&publication_year=2016&pages=5-9&/.
- [38] B. Kaczmarek, Tannic acid with antibacterial activity as a promising component of bio, Mater. -A Minireview, Mater. 13 (14) (2020) 3224, https://doi.org/10.3390/ ma13143224.